Development of inlaid electrodes for whole column electrochemical detection in HPLC

Jung-Ho Seo,[a] Pei Ling Leow,[b] Si-Hyeong Cho,[a] Hyun-Woo Lim,[a] Jin-Young Kim,[ab] Bhavik Anil Patel,[b] Jin-Goo Park*[a] and Danny O'Hare*[b]

Received 15th December 2008, Accepted 1st April 2009
First published as an Advance Article on the web 23rd April 2009
DOI: 10.1039/b822045j

An electrochemical microfluidic device has been fabricated on PET (polyethylene terephthalate) substrate using an imprinting method. The imprinting transfers patterns from a stamp into a substrate mechanically. However, a blanket mould imprinting process has been introduced to embed the photolithographically produced gold metal electrode lines into the PET substrate resulting in an individually addressable array flush to better than 100 nm. The device formed one wall of a packed chromatography column. The array was electrochemically characterised using standard redox probes in both stagnant conditions and under flow. Both numerical modelling and experimental data show improved sensitivity under flow and a limiting current which scaled linearly with the cube root of the volume flow rate. A chromatographic separation of the bioanalytical significant neurotransmitter dopamine (DA) and its metabolite DOPAC was achieved and electrochemically detected at multiple locations within the column. The PET device was stable and robust to leaks to pressures well in excess of those required for chromatographic separations.

1.0 Introduction

Micro total analysis systems (μTAS), also called "lab on a chip (LOC)", integrate analytical processes for sequential operations like sampling, pre-treatment, analytical separation, chemical reaction, analyte detection, and data analysis in a single microfluidic device.[1,2] The aim of this study is to develop a whole in-column electrochemical detection microfluidic device system for liquid chromatography. Several papers have introduced the importance of having whole column detection for separation science.[3–6] The application of novel fabrication methods based upon current MEMS (micro-electro-mechanical systems) technology provide the ideal means to integrate multiple in-column electrochemical detectors within a separation column.

By downsizing the electrodes, the electrochemical response was improved as a lower current leads to smaller errors between the applied and actual voltages caused by voltage drops due to the existence of uncompensated resistance.[7] Besides that, miniaturization of electrochemical microfluidic devices is highly important because of their advantages including low reagent and power consumption, short reaction time, and the portability for parallel operation/integration with other miniaturized devices. Moreover, the favorable area to volume ratio leads to a short diffusion distance of the analytes towards the electrode surface, therefore, providing improved signal to noise ratio, fast response time, enhanced analytical performance and increased sensitivity.[8–10] These characteristics result in more sensitive and rapid detection of biochemical and physiological processes that are essential for basic research as well as for medical applications.

Electrochemical detection has often been used in separation sciences in microfluidic devices due to the ease of control and fabrication.[11–13] The conventional fabrication of electrochemical electrodes was adopted from microelectronics fabrication, such as micromachining, photolithography, injection molding and embossing.[14] Carbon ink working electrodes have been successfully fabricated directly in a capillary electrophoresis separation microchannel using UV laser photoablation.[15,16] The detection of aminophenol and catechol after decoupling the sensor electronics from the separation field. Dong *et al.* have reported on carbon ink which was successfully patterned on polyester substrate (bare PCB board) using screen printing techniques.[17] Besides that, Martin *et al.* successfully inserted a carbon fiber as a working electrode directly into the PDMS microchannel 25 μm before the end of the column.[18] These single electrodes are placed within the channel but towards the end of the separation column due to a high electric field across the column that will interfere with the detection. A paper by Moreira *et al.* has reported integration of a single in in-channel working electrode across an array of channels on PDMS/glass.[19] Electrochemical detections have been widely used within flow channels and many successful numerical models of electrode(s) within microchannel were reported.[20–22]

We proposed the fabrication of inlaid electrodes within the polyethylene terephthalate (PET) substrate of a liquid chromatography (LC) separation column. A series of conventional processes have been carried out such as lift-off technique and chemical mechanical planarization technique. These methods are simple and easy for metal lines patterning. However, these conventional fabrication methods are difficult to achieve on a plastic substrate, as the plastic substrates were often damaged

[a]*Micro Biochip Center, Hanyang University, Ansan, 426-791, Korea. E-mail: jgpark@hanyang.ac.kr; Fax: +82315003452; Tel: +82315003453*
[b]*Department of Bioengineering, Imperial College London, SW7 2AZ London, UK. E-mail: d.ohare@imperial.ac.uk; Fax: +44(0)2075949817; Tel: +44(0)2075945173*

during the fabrication process.[23] An alternative lithography method and novel imprinting procedure is introduced where a mould pattern with a structured topography is transferred into an initially flat polymer film.[24]

In this paper, we describe the use of a blanket mould for the imprinting process to fabricate embedded metal line microelectrodes on a selected plastic substrate, polyethylene terephthalate (PET). A semi-cured thermal bonding technique for the adhesion of the polyester microchannel on the metal lines inlaid PET substrate is used to create the channel and to demonstrate the feasibility of electrochemical detection within an LC column. Numerical models were also reported to prove the feasibility of electrochemical reaction within a packed column.

2.0 Fabrication

Polyethylene terephthalate (PET) ($T_{gPET} = 75$ °C) substrate was used for the fabrication of an electrode embedded electrochemical microfluidic device by a blanket mould imprinting method. PET is better for imprinting as PET is stronger where its tensile strength is higher than PMMA which is 80 MPa and 40 MPa respectively. However, the tensile modulus for PET is up to 4 GPa (Goodfellow Cambridge Ltd.) and PMMA is 1.9 GPa (Smithers Rapra Technology Limited). Therefore, as pressure is applied during insertion of metal lines to the substrate associated with heat PET shows a better outcome in comparison to PMMA where fractures are at a minimum. PET has also shown better adhesion results for embedding metal lines as compared to PMMA during the initial fabrication testing. Fig. 1 shows the flow chart of the fabrication processes of the microfluidic device.

The PET substrate was cleaned in sonicated IPA (isopropyl alcohol). As a microelectrode material Au (2000 Å) film was deposited on PET substrate by a DC magnetron sputtering (SRN610, Sorona Co., Korea). After metal deposition, the microelectrodes were patterned by a wet etching process after conventional photolithography. To embed microelectrodes into the PET substrate, a blanket mould imprinting process was developed. A blanket mould is a non-patterned flat stamp. For an optimal release process between the blanket mould and PET substrate, an anti-adhesion layer was coated on the blanket mould to prevent the polymer from adhering to the mould during the hot embossing imprinting.[25,26] The anti-stiction layer was coated on the blanket mould by a vapour self assembled monolayer method (V-SAM) (VP-SAM, Sorona Co., Korea) with perfluoroctyltrichlorosilane (FOTS, Sigma-Aldrich, USA) as a precursor. Hot embossing (EVG520, EVG, Austria) equipment was used to fabricate an electrochemical microfluidic device which has embedded microelectrodes metal lines in PET (Fig. 2).

Optimized hot embossing imprinting process using blanket mould was achieved at 25 000 N m^{-2} and 80 °C for 90 min. When heated up above the glass transition temperature of the PET substrate, the microelectrodes were pressed into the melted PET substrate. After being cooled down, the blanket mould was separated from the sample and the microelectrodes were successfully embedded into the PET substrate. After the imprinting process, all of the inlaid microelectrodes were observed by an optical microscope (L150A, Nikon, Japan). All of the microelectrodes which have various widths and are spaced from 25 μm to 800 μm were successfully fabricated. Fig. 3 shows the optical image of fabricated electrochemical microfluidic device after the blanket mould imprinting. After the hot embossing process using a blank mould to reversely impress the metal line towards the substrate, the step height difference between the Au electrode and PET was reduced to about 300 Å.

This method produced highly adherent inlaid metal electrodes in PET. The principal advantages of using inlaid electrodes are: (i) improved sealing leading to fewer leaks and greatly increased resistance to pressure, (ii) increased resilience of the electrodes and resistance of peeling and (iii) great improvement of the substrate and electrode adhesion.

The microchannel was cast from a polydimethylsiloxane (PDMS) (Sylgard®) mould using thermoset polyester (TPE) (CFS Fibreglass Supplies). The PDMS mould was prepared from an acrylate master template and was cleaned with sonication in IPA, rinsed with deionised water and dried under a stream of nitrogen gas. Then TPE prepolymer was prepared by adding 0.1 g of hardener to 10 g of TPE resin. The prepolymer was mixed and degassed under vacuum for 2 min to remove dissolved gas in the TPE. The prepolymer was poured onto the PDMS mould and left at room temperature for 2 min. The oven was preheated to 60 °C and the PDMS mould with TPE mixture was semi-cured for 10 min. The semi-cured TPE was left at room temperature for 5 min before peeling off. The TPE microchannel was peeled off using a pair of tweezers and

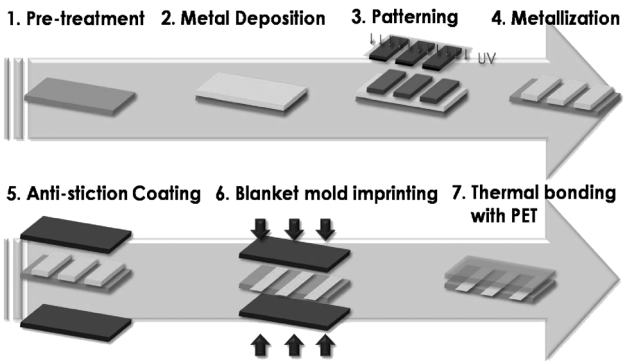

Fig. 1 Fabrication process flow for metal line embedded electrochemical microfluidic device.

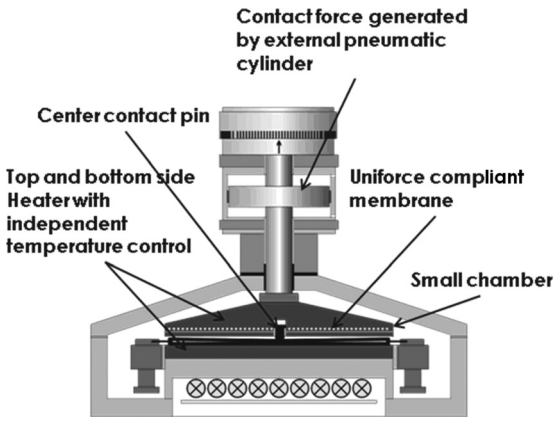

Fig. 2 Schematic of hot embossing imprinting process.

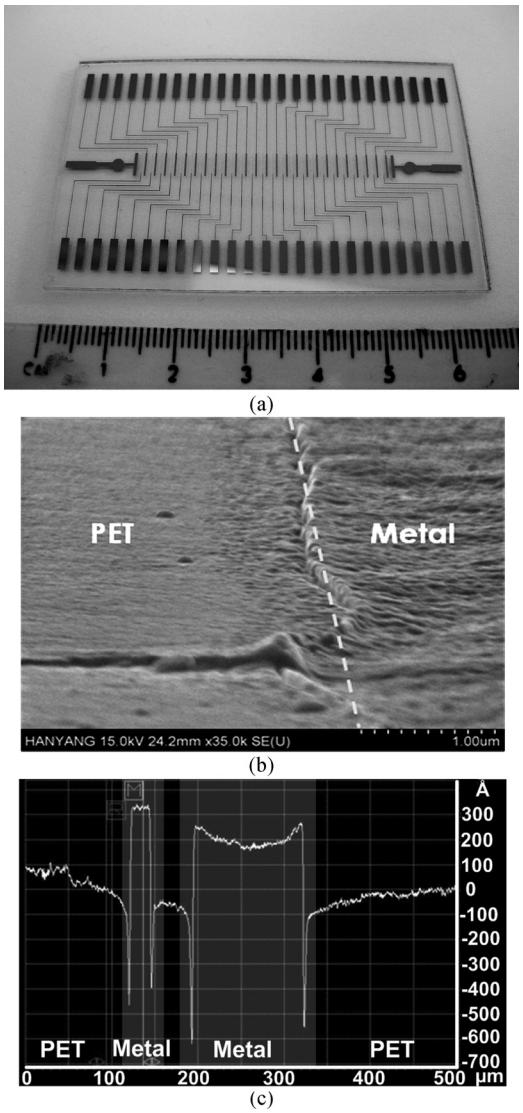

Fig. 3 (a) Photograph of the fabricated metal embedded microfluidic device, (b) SEM image at the interface between Au electrode and PET substrate and (c) the step height between metal electrodes and PET measured by a surface profiler.

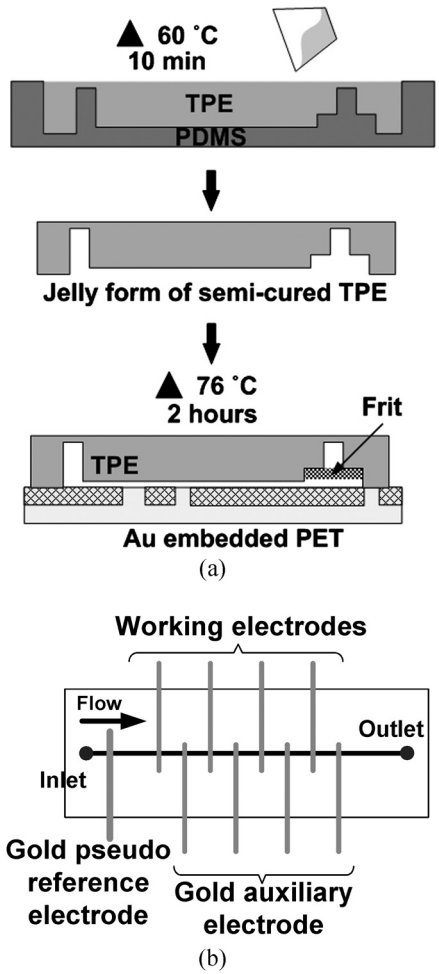

Fig. 4 Schematic for (a) TPE microchannel preparation and adhesion of microchannel and (b) the full device layout with the electrode configuration.

a stainless steel HPLC frit (Phenomenex®) was inserted at the outlet void. The TPE was aligned on the Au embedded PET substrate and using the tweezers, the TPE was gently pressed towards the PET substrate to ensure good adhesion and remove trapped bubbles between the PET substrate and TPE. The whole device was cured for 2 h at 76 °C. Fig. 4 shows the steps for preparing the microchannel.

After the microchannel was fully cured, it was packed with 5 μm octadecyl silane (ODS, Hypersil, Phenomenex®) beads to prepare the chromatography column. The slurry solvent was prepared by suspending 2 mg of ODS into 2 ml of methanol. The slurry solvent was sucked from the outlet of the PET column using a vacuum pump. Fig. 5 shows the close look of the unpacked and packed column of the device.

The strength of the packed PET device under flow was initially accessed by connecting to the HPLC pump. The flow rate was gradually increased from 10 μl min^{-1}–25 μl min^{-1}. At back pressure reading 62 bars, the inlet connector of the PET device was broken and caused disconnection of the pump and device; however, bonding of the microchannel was fine. No leakage was noticed from the bonding of the microchannel and the PET substrate. After resolving the adhesion problem of the external connectors the device can survive up to 90 bars before the bonding of the device broke.

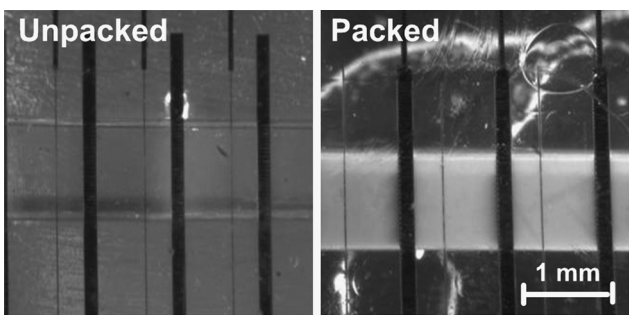

Fig. 5 PET (a) unpacked (b) packed with 5 μm ODS (Phenomenex®).

3.0 Numerical modelling

Numerical models were built to understand the feasibility of electrochemical detection under a partially blocked electrode surface by the ODS sphere particles. A small area of the electrode was built represented by a 3D rectangular block with geometry 10 μm × 10 μm × 5 μm. The bottom boundary of the modelling block was set to act as the electrode. Four 5 μm (diameter) sphere particles were arranged in the block.

The boundary parameter of the electrode was set using the oxidised terms from the Butler–Volmer's flux density, J formulation.

$$J = Fk^0[C_O(0,t)e^{-\alpha f(E-E^{0\prime})} - C_R(0,t)e^{(1-\alpha)f(E-E^{0\prime})}] \quad (1)$$

The k^0 is the standard rate constant (0.001 m s^{-1}), α is the transfer coefficient, $f = F/(RT)$ (V^{-1}), E and $E^{0\prime}$, respectively, are the current and formal potential of an electrode *versus* a reference, and C_O and C_R, respectively are the concentration of the oxidised and reduced species. However, in this model we are only concerned with oxidation of the species.

The distribution of the diffusive flux of the electrode surface with and without sphere particles on top of the electrode is shown in Fig. 6 (a) and (b).

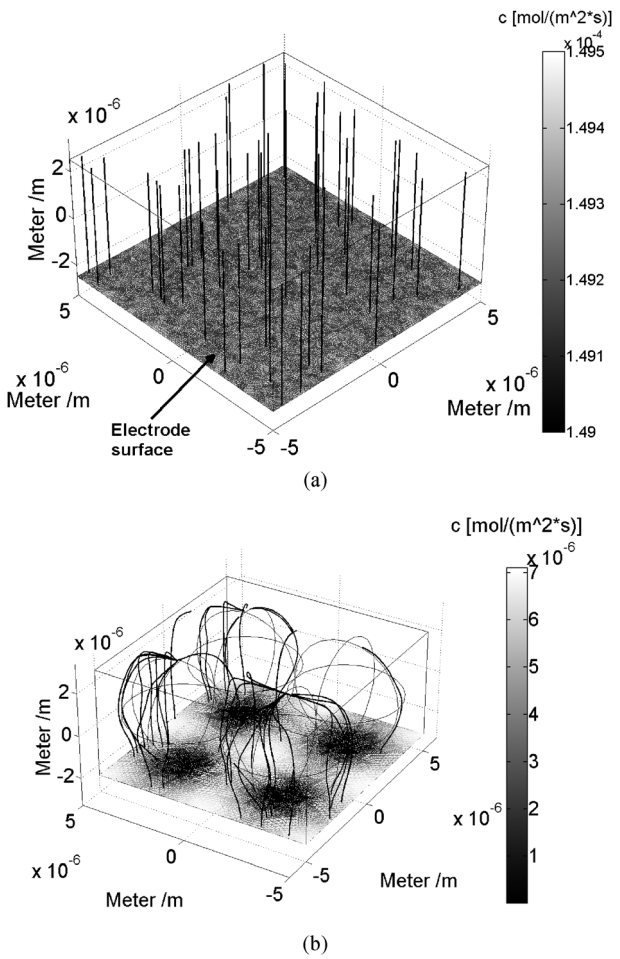

Fig. 6 Diffusive flux distribution under quiescent solution (a) unpacked microchannel (b) packed microchannel with 4 spheres representing the packing material.

Integration of the diffusive flux normal to the electrode surface in quiescent condition shows that diffusive flux to the surface is decreased due to the excluded volume occupied by the spheres. Since the spheres will only have point contact with the surface, to a good approximation, the effects in electron transfer rates, as opposed to mass transport are negligible. Decreased current in quiescent solution in packed columns is therefore expected to be due to a decrease in the effective diffusion coefficient.

Various models exist for the diffusion coefficient in the presence of known fraction volumes of impermeable obstacle that allows prediction of the effective diffusion coefficient. A nearest assumption to support these phenomena was adopted by using Masaro's models of diffusion for polymers[27] using the Mackie and Meares approaches[28] by assuming the current models with and without sphere particle as the resin membrane and the solution in the medium as the electrolyte.

$$\frac{D_{\text{packed}}}{D_{\text{unpacked}}} = \left(\frac{1-\phi}{1+\phi}\right)^{1/2} \quad (2)$$

$$\psi \propto \frac{i}{nFA};$$

$$i \propto D^{1/2}; \text{ from Randles} - \text{Sevčik}$$

$$\frac{i_{\text{packed}}}{i_{\text{unpacked}}} = \frac{\psi_{\text{packed}}}{\psi_{\text{unpacked}}} = \frac{1-\phi}{1+\phi} \quad (3)$$

where the D_{unpacked}, ψ_{unpacked} and i_{unpacked} is the diffusion coefficient, diffusive flux and current in pure solvent respectively and the local diffusion coefficient, D_{packed} and diffusive flux, ψ_{packed} and i_{packed} are decreased in the ratio depending on the volume fraction, φ in the column. The term $(1 - \varphi)$ represented the volume unoccupied by the sphere particles. Volume fraction estimates from eqn 3 using the fluxes calculated (Fig. 6) show good agreement with the exact volume fraction employed in the model. Eqn 3 is therefore entirely consistent with the numerical model. Therefore, we can estimate the volume fraction from the flux or current through the electrode surface in quiescent solution.

Flow velocity, 1 mm s^{-1} was then applied to the same models shown in Fig. 6, the normal diffusive flux plot shows similarity of both models. Fig. 7 shows the top views of these two models.

The normal diffusive flux across the electrode surface is higher as the mass transport on the surface of the electrodes were improved by the applied flow. Higher diffusive flux distributions are noticed near the flow inlet are evenly distributed across the electrode surface. It can be seen in Fig. 7(b) that diffusive flux around the spheres is higher than in the unhindered solution in Fig. 7(a) under flowing conditions.

Numerical models therefore demonstrated the feasibility of electrochemical detections at the wall of a channel packed with spherical stationary phase support.

4.0 Experimental

The HPLC system consisted of an Agilent HP1050 pump, autosampler and column heater. The column was the home-made PET

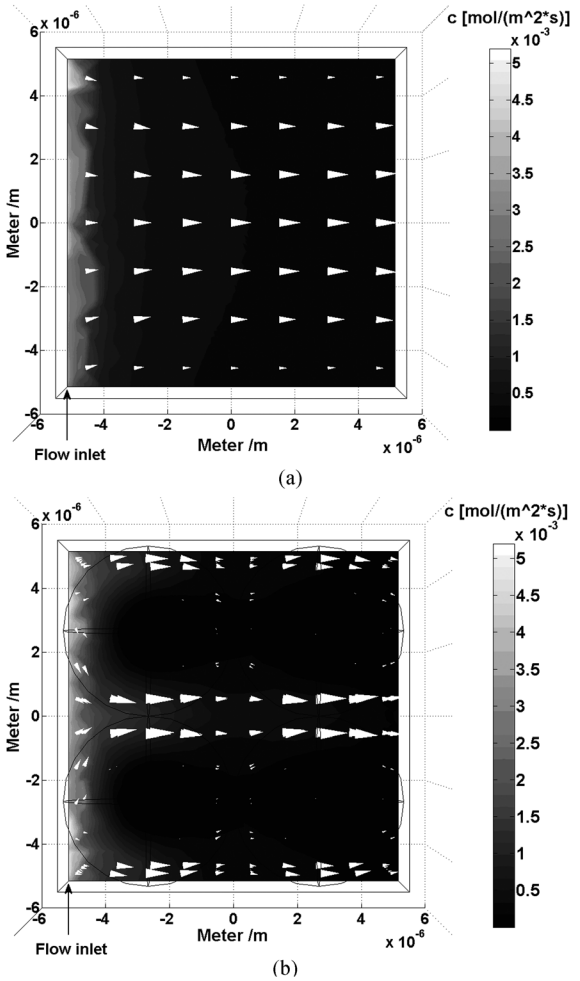

Fig. 7 Top view of normal diffusive flux distribution and flow velocity under flowing solution (a) unpacked microchannel (b) packed microchannel.

column 50.0 mm × 1 mm × 1 mm. Four in-column microband gold electrodes were set at +700 mV with respect to a gold pseudo reference electrode and each paired with a gold auxiliary. These pairing electrodes were 10 mm apart from each other. The potential and current for the in-column detectors were controlled by a CHI potentiostat 1030 (CHI Instruments). The flow rate of the mobile phase was maintained at 80 μl min^{-1} for all experiments and the column temperature was set to 25 ± 0.15 °C.

4.1 Chemicals

Characterization of electrodes. 1 mol dm^{-3} potassium chloride (KCl) from BDH was used as the electrolyte. 1 mmol dm^{-3} potassium ferrocyanide (Fisons scientific, UK) was freshly made in 1 M KCl before the experiments.

In-column electrochemical detection. 3-hydroxytyramine (dopamine, DA) and 3,4-dihydroxyphenylacetic acid (DOPAC) were obtained from Sigma and used as received. All other chemicals used were obtained from VWR International, BDH Prolabo and used as received. All standards were prepared in class A volumetric glassware.

Mobile phase. The citric acid buffer was prepared by dissolving 50 mM sodium citrate in 1 L of deionised water and adjusting to pH 3.2 using concentrated sodium hydroxide. The mobile phase consisted of, stock citric acid buffer (pH 3.2) mixed with UV-grade methanol (HiPerSolv for HPLC, BDH Prolabo) in a ratio of 90 : 10 (v/v) and filtered through a 0.20 μm membrane filter and degassed under vacuum after mixing. Samples were freshly prepared using the citric acid buffer and stored at 4 °C.

4.2 Characterization of in-column electrochemical detection

Two PET columns; packed and unpacked were used for the comparison of the in-column electrochemical detection. Potassium ferrocyanide in 1 M KCl filled up these columns and cyclic voltammetry was carried out on the inlaid electrodes array in quiescent solution. Fig. 8 shows cyclic voltammograms in quiescent 1 mmol dm^{-3} potassium ferrocyanide solution for packed and unpacked channels.

Peak potential width (~60 mv for a reversible process) is unaffected by the packing material, implying no change in electrode kinetics. Peak current however is diminished by 86%. Since, from the Randles–Sevčik equation, peak current scales with $D^{1/2}$ therefore we can use this data in Fig. 8 to calculate the excluded volume fraction. The decrease in peak current implies an effective volume fraction of 0.75 in the packed column.

Since we can record the peak current along the length of the column, longitudinal variation in packing density can be calculated. This is a unique feature of whole column electrochemical detection. Fig. 9 shows the volume fraction in 25 sequential segments. Mean volume fraction is 0.71 ± 0.04 (mean ± standard deviation).

Since linear regression of the data in Fig. 9 gives a straight line with a slope not significantly different for zero (slope = 0.002 ± 0.004 (95% CL)), there is no overall trend in the variation in column packing along its length. This average volume fraction for the column packing is 0.71 which is very near to the

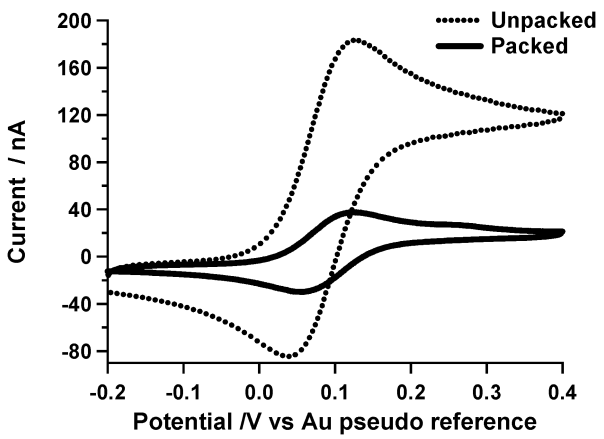

Fig. 8 Cyclic voltammograms: packed and unpacked PET columns under quiescent solution of 1 mmol dm^{-3} potassium ferrocyanide in 1 M KCl.

hexagonal closed-packed which can achieve up to 0.74 packing density. Fig. 10 shows the linear relation of the steady state limiting current for $Fe(CN)_6^{4-}$ *versus* cubic root of the applied flow rates within a packed and unpacked column.

In a flow condition, the electrode current increased with flow rate. According to Compton *et al.*,[29] the limiting current of microband electrodes in a flow channel without packing materials is given by

$$i_{\mathrm{lim-lev}} = 0.925nFc_{\mathrm{bulk}}D^{2/3}V_f^{1/3}(h^2d)^{-1/3}wx_e^{2/3} \quad (4)$$

Where n is the number of electrons transferred, c_{bulk} is the concentration of the bulk solution, V_f is the volume flow rate, h and d are the height and width of the microchannel respectively, x_e is the length of the band electrode.

Current is enhanced for flow in the packed channel compared with the open channel for two reasons. Flow velocities are enhanced in the interstices and increased mixing, due to tortuosity leads to smaller mass transport boundary layers. This is clearly seen in Fig. 10 where current is plotted against $V^{1/3}$. Open channel results are in good agreement with prediction of Compton *et al.*

4.3 In-column electrochemical detections

The in-column electrochemical detections were carried out using four out of 25 electrodes distributed equally across the 50 mm long column, the first electrode was 5 mm away from the inlet and subsequent electrodes were 10 mm apart. The operating potential (+700 mv) for amperometry was determined experimentally from current–voltage curves obtained immediately prior to the separation experiments. Mobile phase was kept at 80 μl min^{-1} and 1 μl of 5 μM samples was injected into the PET packed column. Dopamine was eluted first followed by DOPAC. Fig. 11 shows the in-column electrochemical detection using the fabricated inlaid microband electrodes.

At the first electrode located at the beginning of the separation column, separation of both analytes was not complete. However, at electrode 2 which is located at 15 mm from the inlet shows separation of the 2 analytes. A baseline separation with good separation resolution (R_s) was obtained at electrode 2 where $R_s >$ 1.5. Dopamine peaks were symmetrical from all chromatograms however a tailing effect was observed on the DOPAC from the chromatogram where the tailing factor ranged from 1.7–2.5. The tailing effect noticed on the DOPAC can be greatly reduced by adding ion-pairing agent to the mobile phase.

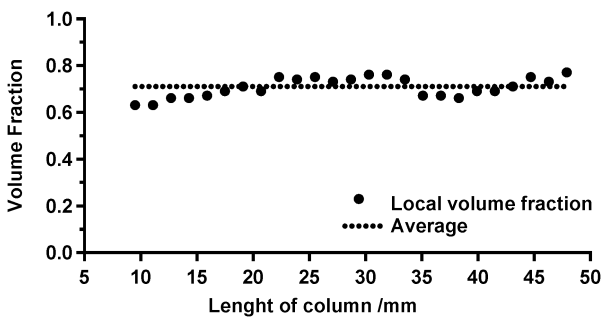

Fig. 9 Volume fraction along the column using standard redox couple $Fe(CN)_6^{4-}$.

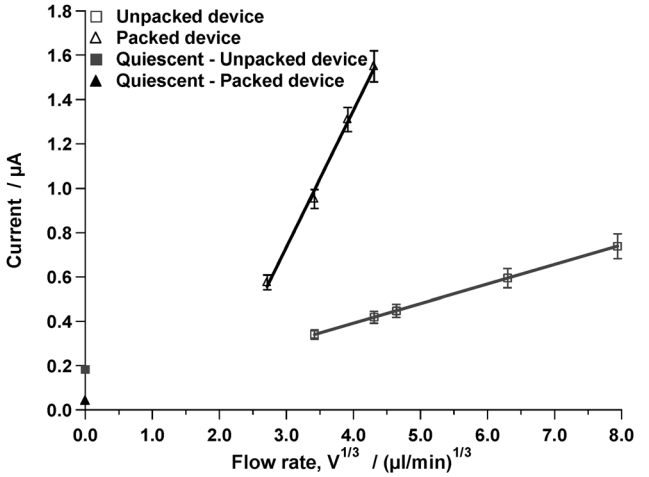

Fig. 10 Average in-column current *versus* cubic root flow rate for unpacked and packed device. No flow results for both devices are also indicated.

5.0 Conclusions

We have demonstrated a fabrication technique for producing electrodes inlaid in a plastic substrate. This overcomes problems of electrodes peeling, flow disturbance, poor adhesion and leaking associated with HPLC in microfabricated channels. The devices were able to tolerate pressures in excess of 90 bars which is more than adequate for HPLC separation. Numerical models showed the feasibility of electrochemical reaction within a packed column. Electrochemical whole column detection

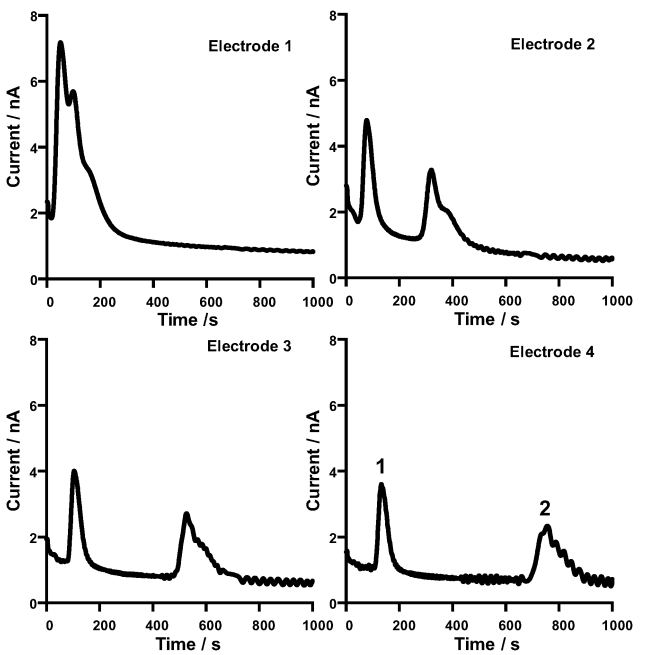

Fig. 11 In-column electrochemical detections for 2 analytes within an LC column; (1) dopamine (2) DOPAC.

allows monitoring of packing efficiency along the length of the column. Calibration showed that electrode current scaled linearly with the cube root of volume flow. Finally, successful separations of a neurotransmitter and its metabolite were demonstrated and the separation could be followed along the column.

6.0 Acknowledgements

This work was financially supported by the Center for Integrated Human Sensing System at Hanyang University. The authors would like to acknowledge Dr James Covington and Mr Fauzan Che Harun from the Sensors Research Laboratory of University of Warwick for assisting in the 3D model fabrication. PL Leow acknowledges Universiti Teknologi Malaysia for the financial support for her research studies. BA Patel acknowledges support provided by an EPSRC LSI Postdoctoral Fellowship Grant.

7.0 Notes and references

1 R. Popovtzer, T. Neufeld, E. z. Ron, J. Rishpon and Y. Shacham-Diamand, *Sens. Actuators, B*, 2006, **119**, 664–672.
2 C. Yi, C.-W. Li, S. Ji and M. Yang, *Anal. Chim. Acta*, 2006, **560**, 1–23.
3 D. G. Gelderloos, K. L. Rowlen and J. W. Birks, *Anal. Chem.*, 1986, **58**, 900–903.
4 K. L. Rowlen, K. A. Duell, J. P. Avery and J. W. Birks, *Anal. Chem.*, 1989, **61**, 2624–2630.
5 J. C. T. Eijkel, Y. C. Kwok and A. Manz, *Lab Chip*, 2001, **1**, 122–126.
6 X.-Z. Wu, T. Huang, Z. Liu and J. Pawliszyn, *TrAC, Trends Anal. Chem.*, 2005, **24**, 369–382.
7 A. J. Bard and L. R. Faulkner, *Electrochemical Methods Fundamentals and Applications*, John Wiley & Son Inc., New York; Chichester, 2001.
8 X. Cai, N. Klauke, A. Glidle, P. Cobbold, G. L. Smith and J. M. Cooper, *Anal. Chem.*, 2002, **74**, 908–914.
9 I. Fritsch and Z. P. Aguilar, *Anal. Bioanal. Chem.*, 2007, **V387**, 159–163.
10 A. M. Bond, *The Analyst*, 1994, **119**, 1R–21R.
11 K. Tóth, K. Stulík, W. Kutner, Z. Fehér and E. Lindner, *Pure Appl. Chem*, 2004, **76**, 1119–1138.
12 L. Nyholm, *The Analyst*, 2005, **130**, 599–605.
13 C. Yi, Q. Zhang, C.-W. Li, J. Yang, J. Zhao and M. Yang, *Anal. Bioanal. Chem.*, 2006, **384**, 1259–1268.
14 S. J. Lee and S. Y. Lee, *Appl. Microbiol. Biotechnol.*, 2004, **64**, 289–299.
15 J. S. Rossier, M. A. Roberts, R. Ferrigno and H. H. Girault, *Anal. Chem.*, 1999, **71**, 4294–4299.
16 J. S. Rossier, R. Ferrigno and H. H. Girault, *J. Electroanal. Chem.*, 2000, **492**, 15–22.
17 H. Dong, C.-M. Li, Y.-F. Zhang, X.-D. Cao and Y. Gan, *Lab Chip*, 2007, **7**, 1752–1758.
18 R. S. Martin, K. L. Ratzlaff, B. H. Huynh and S. M. Lunte, *Anal. Chem.*, 2002, **74**, 1136–1143.
19 N. H. Moreira, A. L. d. J. d. Almeida, M. H. d. O. Piazzeta, D. P. d. Jesus, A. Deblire, A. L. Gobbi and J. A. F. d. Silva, *Lab Chip*, 2009, **9**, 115–121.
20 R. G. Compton, A. C. Fisher, R. G. Wellington, P. J. Dobson and P. A. Leigh, *J. Phys. Chem.*, 1993, **97**, 10410–10415.
21 C. Amatore, N. Da Mota, C. Sella and L. Thouin, *Anal. Chem.*, 2007, **79**, 8502–8510.
22 C. Amatore, N. Da Mota, C. l. Lemmer, C. c. Pebay, C. Sella and L. Thouin, *Anal. Chem.*, 2008, **80**, 9483–9490.
23 N. G. Cha, C. H. Park, K. C. Kim and J. G. Park, *8th Korean MEMS Conference*, 2006, **8**, 685–688.
24 B. D. Gates, Q. Xu, M. Stewart, D. Ryan, C. G. Willson and G. M. Whitesides, *Chem. Rev.*, 2005, **105**, 1171–1196.
25 N. G. Cha, C. H. Park, H. W. Lim and J. G. Park, *J. Korea Phys. Soc.*, 2005, **47**, S530–S534.
26 R. W. Jaszewski, H. Schift, B. Schnyder, A. Schneuwly and P. Gröning, *Appl. Surf. Sci.*, 1999, **143**, 301–308.
27 L. Masaro and X. X. Zhu, *Prog. Polym. Sci.*, 1999, **24**, 731–775.
28 J. S. Mackie and P. Meares, Proc. R. Soc. London, A, 1955, 232, 498–509.
29 M. J. Bidwell, J. A. Alden and R. G. Compton, *J. Electroanal. Chem.*, 1996, **414**, 247–251.

